

Discriminating Non-Isomorphic Graphs with an Experimental Quantum Annealer

Zoe Gonzalez Izquierdo,^{1,2,*} Ruilin Zhou,³ Klas Markström,⁴ and Itay Hen^{1,2}

¹*Department of Physics and Astronomy, and Center for Quantum Information Science & Technology,
University of Southern California, Los Angeles, California 90089, USA*

²*Information Sciences Institute, University of Southern California, Marina del Rey, California 90292, USA*

³*Department of Electrical and Computer Engineering,
Northwestern University, Evanston, Illinois 60208, USA*

⁴*Department of Mathematics and Mathematical Statistics, Umeå University, Umeå, Sweden*

We demonstrate experimentally the ability of a quantum annealer to distinguish between sets of non-isomorphic graphs that share the same classical Ising spectrum. Utilizing the pause-and-quench features recently introduced into D-Wave quantum annealing processors, which allow the user to probe the quantum Hamiltonian realized in the middle of an anneal, we show that obtaining thermal averages of diagonal observables of ‘classically indistinguishable’ non-isomorphic graphs encoded into transverse-field Ising Hamiltonians enable their discrimination. We discuss the significance of our results in the context of the graph isomorphism problem.

I. INTRODUCTION

Commercial quantum annealers [1–3] irrupted into the quantum computing scene about a decade ago, bringing along great promise—and just as much skepticism [4, 5]. Whether these machines do or could in principle provide any advantages over their classical analogues—or whether they could even be considered genuine quantum processors [6–10]—is still a topic of much debate [11–14].

While concrete evidence illustrating their usefulness as practical solvers of optimization problems is still scarce [15, 16] the possibility that they can function as efficient Boltzmann samplers [17–19] or as effective quantum simulators [20–23] has been gaining traction.

Alongside efforts to extend the range of potential applications for quantum annealers, improvements to these devices are continuously being made. Notably, currently available devices allow the user to exercise additional control over various annealing parameters [24] and determine, to a certain extent, the schedule of the anneal, which until recently could only be set to interpolate directly between a transverse-field at the beginning of the anneal and a classical Ising spin glass at the end of it. In particular, novel pause-and-quench capabilities enable some flexibility in determining the rates at which the classical Ising and transverse field Hamiltonians shift their respective strengths. This capability of pausing—the temporary halting of the anneal midway—deployed shortly after the minimum gap, has already been demonstrated to increase the success rates of the quantum annealer when used as an optimizer [18, 25], by giving the system time to thermalize after the minimum gap.

Combining said pause with a sufficiently fast quench to the end of the anneal, such that the evolution during the quench is highly non-adiabatic, allows the user to effectively measure the system at the time of the pause, rendering the annealer a quantum simulator, which pro-

vides access to thermal properties of quantum, rather than classical, Hamiltonians. This new ability has already been tested with varying degrees of success [20–22, 26].

Another novel feature that has recently been introduced into experimental quantum annealers is that of reverse annealing. Here, the initial Hamiltonian is set to be the Ising spin glass and the transverse field is ramped up from zero to some intermediate value, and then brought back to zero again. This capability has been shown to help with the exploitation of regions of interest in the solution space of various optimization problems [27, 28].

In this work, we examine the possibility that mid-anneal probing through pause-and-quench may be utilized toward accomplishing an altogether different enterprise, namely, to solve instances of the Graph Isomorphism problem—the task of deciding whether two graphs are isomorphic (i.e., identical up to vertex relabeling). The possibility of using quantum annealers in this manner was first proposed almost a decade ago [29, 30] and later experimentally attempted with somewhat limited success on an older-generation experimental quantum device that lacked the pause-and-quench features [31].

Here, we study the power of quantum annealers equipped with pause-and-quench capabilities to distinguish between non-isomorphic graphs mapped onto transverse-field Ising Hamiltonians. We find that while measurements at the end of the anneal have only limited discrimination capabilities, mid-anneal measurements allow the extraction of sufficient information from the spectra of strictly quantum Hamiltonians and are in turn powerful enough to distinguish all tested sets of non-isomorphic graphs.

The paper is organized as follows. In Sec. II, we provide some background on the Graph Isomorphism problem, and the means for solving instances of the problem using quantum annealers. Sec. III relays the technical details of our experiments, including information about the specific parameters used. Results are presented and discussed in Sec. IV, and conclusions and final remarks laid out in Sec. V.

* zgonzale@usc.edu

II. DISCRIMINATING BETWEEN GRAPHS USING A QUANTUM ANNEALER

A graph $G = (V, E)$, is a pair of sets, with V being the set of vertices and E the set of edges (unordered pairs of vertices), such that $E \subseteq [V]^2$ [32]. We denote the number of vertices $|V|$ by n . Two graphs G and G' are said to be isomorphic, $G \cong G'$, when there exists a bijection between them that preserves vertex adjacency, that is, one can be converted to the other by a simple relabeling of its vertices.

Determining whether two graphs are isomorphic is known as the Graph Isomorphism (GI) problem [33]. The best general case algorithm for solving it is quasi-polynomial in graph size [34]. One way of solving the GI problem is by comparing graph invariants: maps that take a graph as their argument and assign equal values to isomorphic graphs. A specific method to construct graph invariants results from encoding the structure of the graph on an Ising Hamiltonian [29]. To do this, to every edge (i, j) in the graph we assign a term $\sigma_i^z \sigma_j^z$ in the Hamiltonian, where σ_i^z represents an individual Pauli- z matrix on spin i . Optionally, we can add an external, homogeneous longitudinal field to the spins. We call this the ‘problem Hamiltonian’ of the graph:

$$H_p(G) = \sum_{(i,j) \in E(G)} \sigma_i^z \sigma_j^z + \sum_{i=1}^n \sigma_i^z. \quad (1)$$

The invariant of interest is the spectrum of H_p , and two graphs G and G' are said to be co-Ising if $H_p(G)$ and $H_p(G')$ have the same spectra. The spectrum of H_p is however not a complete invariant, meaning that non-isomorphic, co-Ising graphs exist [35], and trying to use H_p as a graph discriminator to solve the GI problem would therefore fail in the general case.

Quantum annealers offer the exciting possibility of extending the set of Hamiltonian graph invariants into the quantum regime. This can most simply be done by adding a quantum term, such as a homogeneous transverse field, to the classical Ising model onto which the graph is mapped. In this case, the Hamiltonian can be written as

$$H(G, s) = A(s)H_d + B(s)H_p(G), \quad (2)$$

where s is a rescaled, dimensionless time parameter, $s \in [0, 1]$. $A(s)$ and $B(s)$ are functions of s such that $A(0) \gg B(0) \simeq 0$ and $B(1) \gg A(1) \simeq 0$, and H_d is the standard transverse field driver Hamiltonian in quantum annealing:

$$H_d = \sum_{i=1}^n \sigma_i^x. \quad (3)$$

While it is known that there are non-isomorphic graphs for which the spectra of their respective H_p are identical, so far graphs with the same spectra for the full quantum Hamiltonian $H(G, s)$ —quantum co-Ising—which are non-isomorphic are not known to exist.

Calculating the full quantum Ising spectrum of a given graph requires in general the diagonalization of a $2^n \times 2^n$ matrix, which quickly becomes intractable as n increases. Quantum annealers, which implement the above quantum Ising Hamiltonian $H(G, s)$, could alternatively be used to extract valuable information without resorting to calculating its entire spectrum [29]. This can be done if the annealing process is stopped midway at some intermediate s value, $0 < s < 1$, and measurements are then taken in order to obtain an estimation of thermal averages of physical observables.

Experimentally testing the conjecture that physical quantum annealers can distinguish non-isomorphic graphs poses however two main challenges. The first is that currently available processors only allow diagonal measurements to be performed, restricting to some extent the amount of information accessible to the experimenter. Moreover, to ensure that the quantum annealer identifies isomorphic graphs as such, one must also choose to measure quantities that remain unchanged under vertex relabeling.

In this study, we measure the classical energy $E \equiv \langle H_p \rangle$, the z -magnetization $\langle M_z \rangle$, the spin-glass order parameter [29],

$$Q_2 = \sqrt{\frac{1}{N(N-1)} \sum_{i \neq j} \langle \sigma_i^z \sigma_j^z \rangle^2}, \quad (4)$$

and the next-nearest neighbor interaction energy [31]

$$\Omega^2 = \sum_{i,j} [A^2(G)]_{i,j} \sigma_i^z \sigma_j^z. \quad (5)$$

The second challenge that current quantum annealing technology faces is that it only allows measurements to be taken at the end of the anneal, where only the classical H_p component has non-zero strength. This setting is appropriate for the standard usage of a quantum annealer as an optimizer, when the objective is finding the ground state of H_p , and the transverse field is just a means to arriving at it. However, as was discussed above, for distinguishing between non-isomorphic graphs, sampling from a thermal state of a classical Hamiltonian is insufficient in general. To illustrate why this is so, consider Fig. 1, which shows $\Delta E = E_{G13} - E_{G13p}$ for one of the pairs of graphs we try to distinguish, denoted $G13$ and $G13p$, with $n = 13$ (small enough to be directly diagonalized). These graphs are indistinguishable at the end of the anneal as evidenced by the $\Delta E = 0$ at $s = 1$ (as well as in the $s = 0$ limit when their Hamiltonians are both only the transverse field), and the difference between them is pronounced enough only well within the quantum regime. A measurement near $s = 0.3$, where ΔE peaks, would thus be ideal for distinguishing them. The inability of sampling from a classical Hamiltonian to discriminate non-isomorphic graphs was also demonstrated in Ref. [31]. There, the authors tested whether an experimental quantum annealer could lead to distin-

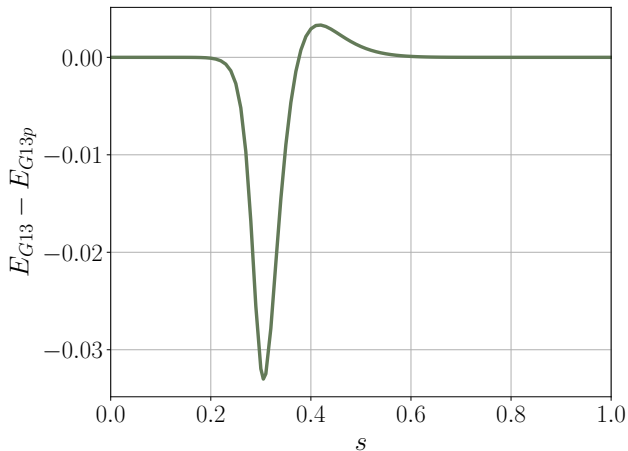


FIG. 1. Difference in classical energy $E = \langle H_p \rangle$ throughout the anneal at $T = 12\text{mK}$ (device operating temperature) for the smallest pair of graphs we test, G_{13} and G_{13p} .

guishable statistics when measuring only at the end of the anneal, concluding this cannot be done in general.

While currently available hardware still only allows $s = 1$ measurements, mid-anneal differences may be captured thanks to the newly added capability of employing fast quenches [18, 20, 21, 36]. These in turn induce highly non-adiabatic transitions. While still far from being the ideal instantaneous quench (which is equivalent to a mid-anneal measurement), fast quenches allow, to some extent, access to information about the spectra of the quantum graph Hamiltonians. As we demonstrate below, combining these fast quenches with reverse annealing and pausing can be used to substantially increase the distinguishability power of quantum annealers.

III. METHODS

The quantum annealing processor we use in our experiment is the D-Wave 2000Q quantum annealer located at NASA Ames Research Center. Released in 2016, its 2048 qubit chip has a 16×16 -cell Chimera connectivity. Chimera graphs of size s (C_s), consist of s^2 Chimera cells arranged in a square pattern. Each Chimera cell is a complete bipartite graph with 8 vertices, or $K_{4,4}$. Each vertex is connected to 4 others within the cell, and also to 2 more outside the cell (except for cells on the boundaries). Each edge can be assigned a coupling strength J_{ij} and each qubit a longitudinal field h_i .

Every graph G we test is mapped to a problem Hamiltonian H_p as given in Eq. (1). Each graph vertex is represented by a qubit on the chip, and each edge of the graph is assigned the appropriate coupler with strength $J_{ij} = 1$ (non-edge couplers are set to 0). The particular choice of physical qubits and couplers representing the logical graph is what we refer to as embedding. In gen-

eral, there will be numerous possible embedding choices for each graph. In addition, we apply a homogeneous external longitudinal field on all qubits, with $h_i = 1 \forall i$. We also perform gauge averaging to mitigate potential intrinsic biases in the physical components. This is done by repeating each run several times, each applying a different random transformation to the couplers and longitudinal fields of the form $J_{ij} \rightarrow a_i a_j J_{ij}$, $h_i \rightarrow a_i h_i$, with $a_i \in \{-1, +1\}$. These are unitary transformations that leave the energy spectrum unchanged, and the solution to the original problem can be easily recovered from that of the gauge-transformed problem by reversing the transformation.

In our annealing procedure, we employ a reverse annealing protocol with a pause, followed by a quench. With reverse annealing, $s(t = 0) = 1$ and the initial Hamiltonian is $H(s = 1) \approx H_p$. The system is prepared in a classical state set by the user (in our case, all spins up), and the anneal starts ‘in reverse’ (i.e. decreasing s) to some intermediate value $s = s_p$. The same path must then be traced back, as the process is required to end at $s = 1$. In our case we also choose to introduce a pause of length t_p at s_p . A qualitative depiction of our schedule is shown in Fig. 2. After the first anneal is completed, one can choose to either reinitialize to the chosen classical state, or take the final state for each anneal as the initial state for the next. We choose the latter option.

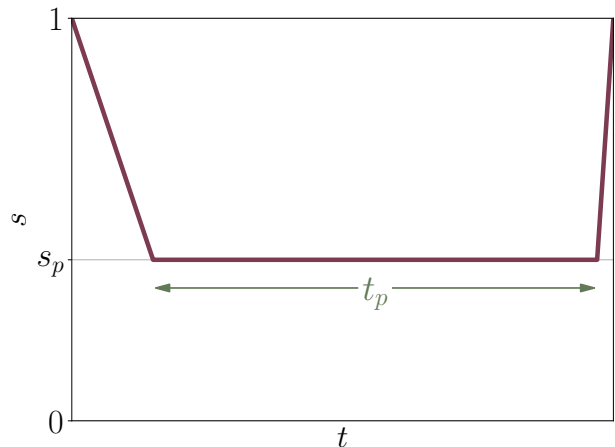


FIG. 2. Diagram of the annealing schedule $s(t)$ for reverse annealing with a pause and a final quench (not to scale). The system is initialized at $s = 1$, annealed back to an intermediate s_p , paused for a time t_p and finally annealed to $s = 1$ again, this time at the maximum rate.

In our runs, the duration of the reverse part of the anneal as well as the pause are set constant (at $1\mu\text{s}$ and $100\mu\text{s}$, respectively), as is the rate of the quench (the fastest possible, $1\mu\text{s}^{-1}$). The location of the pause s_p is varied in $[0.1, 0.2, \dots, 0.9]$ to obtain statistics at different points in the anneal. This schedule is designed to allow us to tap into the quantum spectrum of the Hamiltonian at the time of the pause s_p , by letting the system relax

to the thermal state of $H(s_p)$ while also trying to prevent further thermalization during the quench. Rather than obtaining the ground state (or thermal distribution) of H_p as we would for optimization purposes, here we are interested in obtaining configurations whose statistics retain information about the state of the system at s_p where the Hamiltonian is non-classical.

Recent results [26] suggest that the current fastest rate for the quench is, in general, not sufficiently fast to fully prevent the state from changing during the quest, and thus measurements might not faithfully represent the thermal state at $H(s_p)$. For our purpose, the requirement that the state remains unchanged during the quench is however not strictly necessary. We only require that enough information is preserved during the quench so that the differences between quantum spectra are not completely washed out by the time a measurement is taken at the end of the anneal.

For each graph and pause location, we choose 200 random gauges and perform 1000 anneals per gauge, obtaining 200,000 final configurations per set of parameters. Diagonal observables—classical energy $\langle H_p \rangle$, magnetization $\langle M_z \rangle$, spin-glass order parameter Q_2 and next-nearest neighbor interaction Ω^2 (defined in Sec. II)—are calculated for each gauge, and then a bootstrap over the gauges is performed and the mean and 95% confidence interval values reported.

To ensure that the annealer does not falsely distinguish isomorphic graphs, and that differences in results stem in fact from non-isomorphism, rather than biases or noise, we test isomorphic graphs as well, as a baseline. This is done in one of two ways: in the case of pairs of graphs that can be embedded using the same qubits, a third graph, also defined on the same set of qubits and isomorphic to the first, is tested alongside the pair. Isomorphic variants are easily generated by random relabelings of graph vertices. We note that since the choice of embedding is limited by the rigid, sparse connectivity of the Chimera layout, embedding on the same qubits is not always possible. When that is the case, we do not compare a single embedding choice for each graph, due to the fact that different physical qubits and couplers might suffer from intrinsic biases. Instead, each graph is assigned several different embeddings, and results are averaged over those. We find that the differences between non-isomorphic graphs remain statistically significant even averaging over several different embeddings.

IV. RESULTS

To test the extent to which quantum annealing processors can discriminate ‘classically indistinguishable’ non-isomorphic graphs, we consider several sets of graphs of varying sizes (ranging between $n = 13$ and $n = 33$ vertices). These graphs are specially constructed to be classically co-Ising and native to the Chimera architecture (the reader is referred to the Appendix for details on the

construction process and the particulars of the graphs tested). Importantly, to verify that the experimental an-

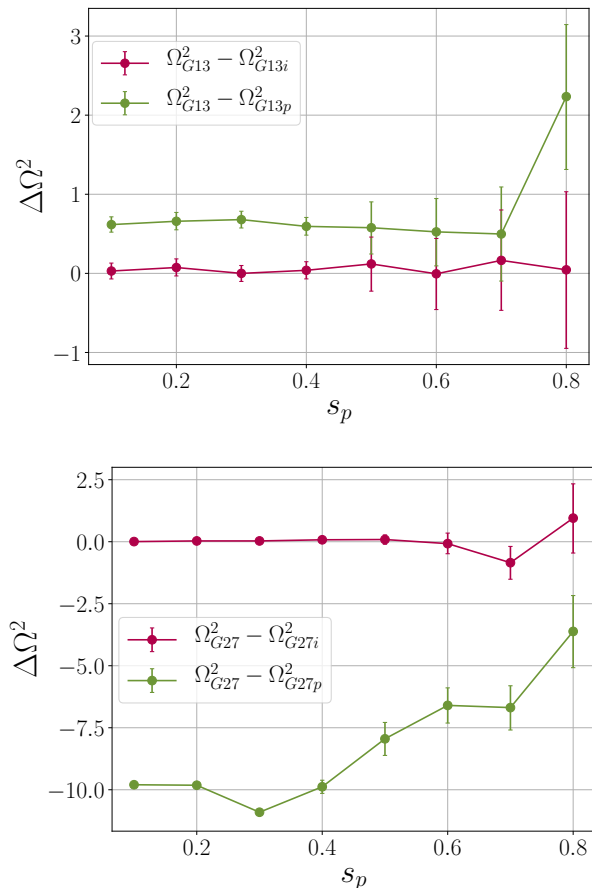


FIG. 3. Differences in next-nearest neighbor interaction energy as a function of the pause point s_p . $\langle \Omega^2 \rangle$ suffices to discriminate between $G13$ and $G13p$ (top) and between $G27$ and $G27p$ (bottom). The red line shows the difference between the two isomorphic graphs $G13$ and $G13i$ (top) and $G27$ and $G27i$ (bottom), staying relatively constant around 0, while the green line represents the difference between the non-isomorphic graphs $G13$ and $G13p$ (top) and $G27$ and $G27p$ (bottom), which remains non-zero throughout. Error bars show the 95% confidence interval after performing a bootstrap over the 200 gauges.

nealer does not falsely distinguish isomorphic graphs as well, we add to each set of non-isomorphic graphs we wish to discriminate isomorphic variants of some of the graphs. When the set is a pair that can be embedded using the same set of qubits, two sets of data are presented for each observable: the difference in the observable between the two isomorphic graphs—which should be zero (up to statistical errors) if the annealer sees them as such—and the difference in the observable between the non-isomorphic graphs—which indicates that the annealer tells them apart if the value is non-zero. When the graphs within a set cannot be embedded using the same set of qubits, we average over equivalent embeddings.

To successfully distinguish non-isomorphic graphs, differences in the observables must be larger than the variation across embeddings. We find that in the regions where differences are most pronounced, the difference in observable averages is typically an order of magnitude greater than the error bars which represent variations across embeddings. We next report our main findings.

We first discuss the two pairs of graphs previously tested in Ref. [31]. There, an $n = 13$ -vertex pair of graphs was distinguished by examining sorted individual values of a triplet of observables, while for the larger pair (with $n = 27$) the two graphs could not be told apart. Using a mid-anneal pause, which allows us to probe quantum Hamiltonians in the middle of the anneal, we are able to measure the differences in the quantum spectra for both pairs of graphs, and to do so simply from the outcome of a single diagonal observable, such as $\langle H_p \rangle$, Q_2 , $\langle M_z \rangle$ or $\langle \Omega^2 \rangle$.

The above pairs of graphs have the advantage that they could be embedded using the same set of qubits on the annealer hardware. To ensure that we are in fact measuring differences in quantum spectra, rather than differences caused by noise or other factors, we also test a third graph alongside each pair, that is isomorphic to one of the two. We find the quantum annealer is unable to ‘distinguish’ between the isomorphic graphs, as should be the case. Plots depicting the measured differences for the $n = 13$ pair and for the previously indistinguishable $n = 27$ pair are shown in Fig. 3.

We next examine new tuples of graphs designed to be classically co-Ising, native to the Chimera architecture, as detailed in the Appendix, and have the added difficulty that they cannot in general be embedded using the same sets of qubits. We examine in particular a pair with $n = 17$ vertices and two sets of four graphs of sizes $n = 25$ and $n = 33$.

To confirm that any measured differences are in fact due to non-isomorphicity, we run several different embeddings for each of these graphs, and average the measurement outcomes over the embeddings of each graph. Ideally, we expect to obtain similar outcomes for different embeddings of same graphs. Indeed, this is what we find. Figure 4 (left) depicts the distinguishability power of the experimental quantum annealer for the $n = 17$ pair of graphs. Here, we pick the spin-glass order parameter Q_2 as the discriminator of choice. In Fig. 4 (middle) we show how, for a 4-tuple of graphs of size $n = 25$, pausing in a region in the middle of the anneal brings out the differences in the quantum spectra between the four graphs, which are much larger than the small deviations due to the different embeddings. We similarly test another 4-tuple with $n = 33$ (Fig. 4 right).

As is evident from these figures, differences between the tested sets of non-isomorphic graphs are most pronounced in the region where s is far from the ends of the anneal, well into the ‘quantum regime’. In the limit of $s \approx 1$, no differences are present as our graphs are specially constructed to be classically co-Ising. In the

other limit $s \approx 0$, no differences should be detected because only the H_d component, which is identical across all graphs, has non-zero strength. Interestingly, we find that in practice, as is evident from the bottom panel of Fig. 3, outcomes from the non-isomorphic graphs can be quite different even when the pause is rather close to $s = 0$. One plausible explanation for the above observation is that for pauses that take place at small s values, the quench to $s = 1$ cannot be performed fast enough to preserve the state of the system at the pause point. This is expected since for small s values the quench has to pass through the minimum gap, in the vicinity of which thermalization processes take place at very rapid rates [18].

V. CONCLUSIONS AND OUTLOOK

We presented results demonstrating the ability of an experimental quantum annealer to solve instances of the graph isomorphism problem. We illustrated that a physical quantum annealer’s ability to distinguish between ‘classically indistinguishable’ graphs—graphs whose classical Ising spectra are identical—may be accomplished by utilizing pause-and-quench features, which allow the user to probe the thermal properties of strictly quantum Hamiltonians; capabilities that have so far been out of reach for standard annealing processors. We also showed that while measurements at the end of the evolution following a standard annealing protocol are not able to distinguish between non-isomorphic graphs, introducing a mid-anneal pause followed by a fast quench allowed us to access properties of strictly quantum Hamiltonians, providing the annealer the necessary distinguishability power that standard annealing protocols lack.

We confirmed the robustness of our technique across different graph choices and native embeddings, as a crucial first step in the quest to expand the scope of this method. With the advent of new architectures with increased connectivity that will soon succeed the Chimera architecture of current D-Wave devices, the pool of native graphs is expected to expand significantly. For larger, more connected graphs, being able to rely on heuristic methods for embedding-finding will likely be necessary, and the success of this method relies on the consistency of results across embeddings.

We found that despite pause-and-quench being far from a perfect mechanism to substitute a measurement in the middle (as quench times cannot be made arbitrarily short and pause times cannot be made arbitrarily long) [26], the method we employed performed as intended insofar as extracting sufficient information about the differences in the quantum spectra of non-isomorphic graphs at the time of the pause. We expect that further improvements in technology, e.g., a faster quench or, better yet, novel mechanisms for taking measurements in the region $0 < s < 1$, would lead to results that capture the quantum spectrum more faithfully, enhancing the annealer’s discriminating capabilities. Nonetheless, the

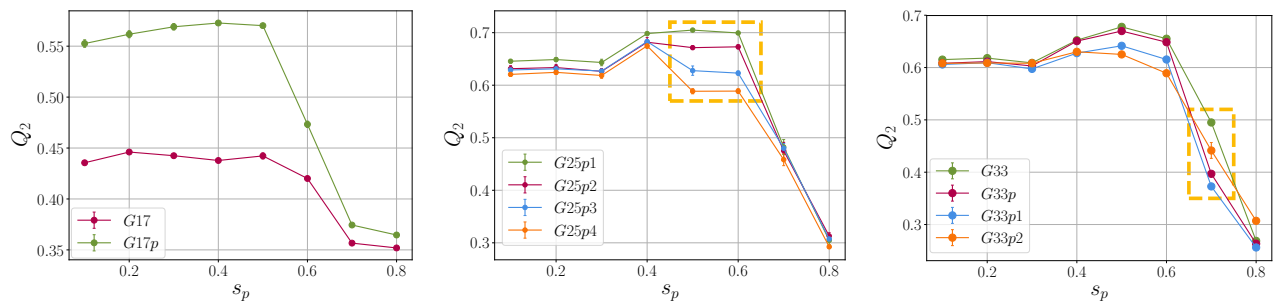


FIG. 4. **Left:** The spin-glass order parameter Q_2 as a function of pause point s_p . Measurements of Q_2 can distinguish between $G17$ and $G17p$. Data points are averaged over 5 different embeddings, with error bars showing the standard error. **Middle:** A group of four classically equivalent graphs with $n = 25$ becomes distinguishable when probing the quantum regime mid-anneal. If the pause is too early or too late, we are not able to measure the differences across these four graphs. Each data point is averaged over 5 different embeddings, with error bars showing the standard error of the mean. Individual embedding results were first calculated using a bootstrap over the 200 gauges. The differences between the four graphs are most pronounced in the range $s \in [0.5, 0.6]$ (marked by the dashed contour). **Right:** Similar to the $n = 25$ tuple, Q_2 can distinguish all four $G33$ graphs with a pause around $s_p = 0.7$.

current setup proved sufficient to distinguish all tested sets of graphs by estimating thermal averages of one or several physical (diagonal) observables, where at least one of them—and usually more—show statistically significant differences between the non-isomorphic graphs. This brings to fruition the idea, proposed almost a decade ago [29], that classically co-spectral graphs could be distinguished by a quantum annealer via measurements of their quantum properties.

Importantly, in this work we have not discussed the time resources needed for quantum-assisted graph discrimination, nor did we discuss the potential of observing quantum speedups, which remains an interesting consideration to be addressed in future work. While the present study focuses on feasibility, a rigorous investigation of performance and its scaling with the size of the graphs will be necessary to test this method against classical algorithms. Differences between reverse and forward annealing with a pause should be considered, including the

duration of the pause, as well as other annealing parameters, adjusted to minimize time-to-solution.

ACKNOWLEDGMENTS

This research is based upon work (partially) supported by the Office of the Director of National Intelligence (ODNI), Intelligence Advanced Research Projects Activity (IARPA), via the U.S. Army Research Office contract W911NF-17-C-0050. Klas Markström was supported by The Swedish Research Council grant 2014-4897. The views and conclusions contained herein are those of the authors and should not be interpreted as necessarily representing the official policies or endorsements, either expressed or implied, of the ODNI, IARPA, or the U.S. Government. The U.S. Government is authorized to reproduce and distribute reprints for Governmental purposes notwithstanding any copyright annotation thereon.

-
- [1] R. Harris, J. Johansson, A. J. Berkley, M. W. Johnson, T. Lanting, Siyuan Han, P. Bunyk, E. Ladizinsky, T. Oh, I. Perminov, E. Tolkacheva, S. Uchaikin, E. M. Chapple, C. Enderud, C. Rich, M. Thom, J. Wang, B. Wilson, and G. Rose, “Experimental demonstration of a robust and scalable flux qubit,” *Phys. Rev. B* **81**, 134510 (2010), [arXiv:0909.4321](https://arxiv.org/abs/0909.4321) [cond-mat.supr-con].
- [2] R. Harris, M. W. Johnson, T. Lanting, A. J. Berkley, J. Johansson, P. Bunyk, E. Tolkacheva, E. Ladizinsky, N. Ladizinsky, T. Oh, F. Cioata, I. Perminov, P. Spear, C. Enderud, C. Rich, S. Uchaikin, M. C. Thom, E. M. Chapple, J. Wang, B. Wilson, M. H. S. Amin, N. Dickson, K. Karimi, B. MacReady, C. J. S. Truncik, and G. Rose, “Experimental investigation of an eight-qubit unit cell in a superconducting optimization processor,” *Phys. Rev. B* **82**, 024511 (2010), [arXiv:1004.1628](https://arxiv.org/abs/1004.1628) [cond-mat.supr-con].
- [3] Mark Johnson, Mohammad Amin, S Gildert, Trevor Lanting, F Hamze, N Dickson, R Harris, Andrew Berkley, J Johansson, Paul Bunyk, E Chapple, C Enderud, Jeremy Hilton, Kamran Karimi, E Ladizinsky, Nicolas Ladizinsky, T Oh, I Perminov, C Rich, and Geordie Rose, “Quantum annealing with manufactured spins,” *Nature* **473**, 194–8 (2011).
- [4] Wim van Dam, Michele Mosca, and Umesh Vazirani, “How Powerful is Adiabatic Quantum Computation?” arXiv e-prints, quant-ph/0206003 (2002), [arXiv:quant-ph/0206003](https://arxiv.org/abs/quant-ph/0206003) [quant-ph].
- [5] Marko Žnidarič and Martin Horvat, “Exponential complexity of an adiabatic algorithm for an NP-complete problem,” *Phys. Rev. A* **73**, 022329 (2006), [arXiv:quant-ph/0509162](https://arxiv.org/abs/quant-ph/0509162) [quant-ph].
- [6] Sergio Boixo, Tameem Albash, Federico Spedalieri,

- Nicholas Chancellor, and Daniel Lidar, “Experimental signature of programmable quantum annealing,” *Nature communications* **4**, 2067 (2013).
- [7] Sergio Boixo, Troels Frimodt Rønnow, Sergei Isakov, Zhihui Wang, David Wecker, Daniel Lidar, John Martinis, and Matthias Troyer, “Quantum annealing with more than one hundred qubits,” *Nat Phys* **10** (2013), [10.1038/nphys2900](https://doi.org/10.1038/nphys2900).
- [8] John Smolin and Graeme Smith, “Classical signature of quantum annealing,” *Frontiers in Physics* **2** (2013), [10.3389/fphy.2014.00052](https://doi.org/10.3389/fphy.2014.00052).
- [9] Seung Shin, Graeme Smith, John Smolin, and Umesh Vazirani, “How “quantum” is the d-wave machine?” (2014).
- [10] Tameem Albash, Walter Vinci, Anurag Mishra, Paul Warburton, and Daniel Lidar, “Consistency tests of classical and quantum models for a quantum annealer,” *Physical Review A* **91**, 042314 (2015).
- [11] Troels F. Rønnow, Zhihui Wang, Joshua Job, Sergio Boixo, Sergei V. Isakov, David Wecker, John M. Martinis, Daniel A. Lidar, and Matthias Troyer, “Defining and detecting quantum speedup,” *Science* **345**, 420–424 (2014), <https://science.sciencemag.org/content/345/6195/420.full.pdf>.
- [12] Victor Martin-Mayor and Itay Hen, “Unraveling quantum annealers using classical hardness,” *Scientific Reports* **5** (2015), [10.1038/srep15324](https://doi.org/10.1038/srep15324).
- [13] Salvatore Mandr, Helmut Katzgraber, and Creighton Thomas, “The pitfalls of planar spin-glass benchmarks: Raising the bar for quantum annealers (again),” *Quantum Science and Technology* **2** (2017), [10.1088/2058-9565/aa7877](https://doi.org/10.1088/2058-9565/aa7877).
- [14] Salvatore Mandr and Helmut Katzgraber, “A deceptive step towards quantum speedup detection,” *Quantum Science and Technology* **3** (2017), [10.1088/2058-9565/aac8b2](https://doi.org/10.1088/2058-9565/aac8b2).
- [15] Itay Hen, Joshua Job, Tameem Albash, Troels Frimodt Rønnow, Matthias Troyer, and Daniel Lidar, “Probing for quantum speedup in spin glass problems with planted solutions,” *Physical Review A* **92** (2015), [10.1103/PhysRevA.92.042325](https://doi.org/10.1103/PhysRevA.92.042325).
- [16] Helmut Katzgraber, Firas Hamze, Zheng Zhu, Andrew Ochoa, and Humberto Munoz-Bauza, “Seeking quantum speedup through spin glasses: The good, the bad, and the ugly,” *Physical Review X* **5** (2015), [10.1103/PhysRevX.5.031026](https://doi.org/10.1103/PhysRevX.5.031026).
- [17] Mohammad H. Amin, Evgeny Andriyash, Jason Rolfe, Bohdan Kulchyt'sky, and Roger Melko, “Quantum boltzmann machine,” *Phys. Rev. X* **8**, 021050 (2018).
- [18] Jeffrey Marshall, Davide Venturelli, Itay Hen, and Eleanor G. Rieffel, “The power of pausing: advancing understanding of thermalization in experimental quantum annealers,” arXiv e-prints , arXiv:1810.05881 (2018), [arXiv:1810.05881 \[quant-ph\]](https://arxiv.org/abs/1810.05881).
- [19] Richard Y. Li, Tameem Albash, and Daniel A. Lidar, “Improved Boltzmann machines with error corrected quantum annealing,” arXiv e-prints , arXiv:1910.01283 (2019), [arXiv:1910.01283 \[quant-ph\]](https://arxiv.org/abs/1910.01283).
- [20] Andrew King, Juan Carrasquilla, Isil Ozfidan, Jack Raymond, Evgeny Andriyash, Andrew Berkley, Mauricio Reis, Trevor M. Lanting, Richard Harris, Gabriel Poulin-Lamarre, Anatoly Yu. Smirnov, Christopher Rich, Fabio Altomare, Paul Bunyk, Jed Whittaker, Loren Swenson, Emile Hoskinson, Yuki Sato, Mark H. Volkmann, and Mohammad Amin, “Observation of topological phenomena in a programmable lattice of 1,800 qubits,” *Nature* **560** (2018), [10.1038/s41586-018-0410-x](https://doi.org/10.1038/s41586-018-0410-x).
- [21] R. Harris, Y. Sato, A. J. Berkley, M. Reis, F. Altomare, M. H. Amin, K. Boothby, P. Bunyk, C. Deng, C. Enderud, S. Huang, E. Hoskinson, M. W. Johnson, E. Ladizinsky, N. Ladizinsky, T. Lanting, R. Li, T. Medina, R. Molavi, R. Neufeld, T. Oh, I. Pavlov, I. Perminov, G. Poulin-Lamarre, C. Rich, A. Smirnov, L. Swenson, N. Tsai, M. Volkmann, J. Whittaker, and J. Yao, “Phase transitions in a programmable quantum spin glass simulator,” *Science* **361**, 162–165 (2018), <http://science.sciencemag.org/content/361/6398/162.full.pdf>.
- [22] Andrew D. King, Jack Raymond, Trevor Lanting, Sergei V. Isakov, Masoud Mohseni, Gabriel Poulin-Lamarre, Sara Ejtemaee, William Bernoudy, Isil Ozfidan, Anatoly Yu. Smirnov, Mauricio Reis, Fabio Altomare, Michael Babcock, Catia Baron, Andrew J. Berkley, Kelly Boothby, Paul I. Bunyk, Holly Christiani, Colin Enderud, Bram Evert, Richard Harris, Emile Hoskinson, Shuiyuan Huang, Kais Jooya, Ali Khodabandelou, Nicolas Ladizinsky, Ryan Li, P. Aaron Lott, Allison J. R. MacDonald, Danica Marsden, Gaelen Marsden, Teresa Medina, Reza Molavi, Richard Neufeld, Mana Norouzpour, Travis Oh, Igor Pavlov, Ilya Perminov, Thomas Prescott, Chris Rich, Yuki Sato, Benjamin Sheldan, George Sterling, Loren J. Swenson, Nicholas Tsai, Mark H. Volkmann, Jed D. Whittaker, Warren Wilkinson, Jason Yao, Hartmut Neven, Jeremy P. Hilton, Eric Ladizinsky, Mark W. Johnson, and Mohammad H. Amin, “Scaling advantage in quantum simulation of geometrically frustrated magnets,” arXiv e-prints , arXiv:1911.03446 (2019), [arXiv:1911.03446 \[quant-ph\]](https://arxiv.org/abs/1911.03446).
- [23] Yuki Bando, Yuki Susa, Hiroki Oshiyama, Naokazu Shibata, Masayuki Ohzeki, Fernando Javier Gómez-Ruiz, Daniel A. Lidar, Adolfo del Campo, Sei Suzuki, and Hidetoshi Nishimori, “Probing the Universality of Topological Defect Formation in a Quantum Annealer: Kibble-Zurek Mechanism and Beyond,” arXiv e-prints , arXiv:2001.11637 (2020), [arXiv:2001.11637 \[quant-ph\]](https://arxiv.org/abs/2001.11637).
- [24] “Technical description of the d-wave quantum processing unit,” D-Wave User Manual 09-1109A-R (2020).
- [25] G. Passarelli, V. Cataudella, and P. Lucignano, “Improving quantum annealing of the ferromagnetic p -spin model through pausing,” *Phys. Rev. B* **100**, 024302 (2019).
- [26] Z. Gonzalez Izquierdo, T. Albash, and I. Hen, “Testing a quantum annealer as a quantum thermal sampler,” arXiv e-prints , arXiv:2003.00361 (2020), [arXiv:2003.00361 \[quant-ph\]](https://arxiv.org/abs/2003.00361).
- [27] Davide Venturelli and Alexei Kondratyev, “Reverse quantum annealing approach to portfolio optimization problems,” *Quantum Machine Intelligence* , 17–30 (2019).
- [28] Masaki Ohkuwa, Hidetoshi Nishimori, and Daniel A. Lidar, “Reverse annealing for the fully connected p -spin model,” *Phys. Rev. A* **98**, 022314 (2018).
- [29] Itay Hen and A. P. Young, “Solving the graph-isomorphism problem with a quantum annealer,” *Phys. Rev. A* **86**, 042310 (2012).
- [30] Frank Gaitan and Lane Clark, “Graph isomorphism and adiabatic quantum computing,” *Physical Review A* **89**, 022342 (2014), [arXiv:1304.5773 \[quant-ph\]](https://arxiv.org/abs/1304.5773).
- [31] Walter Vinci, Klas Markström, Sergio Boixo, Aidan Roy, Federico M. Spedalieri, Paul A. Warburton, and Simone

- Severini, “Hearing the Shape of the Ising Model with a Programmable Superconducting-Flux Annealer,” *Scientific Reports* **4**, 5703 (2014), arXiv:1307.1114 [quant-ph].
- [32] Reinhard Diestel, *Graph Theory (Graduate Texts in Mathematics)*, 5th ed. (Springer, 2016).
- [33] Johannes Köbler, Uwe Schöning, and Jacobo Torán, *The Graph Isomorphism Problem: Its Structural Complexity* (Birkhauser Verlag, 1994).
- [34] László Babai, “Graph Isomorphism in Quasipolynomial Time,” arXiv e-prints, arXiv:1512.03547 (2015), arXiv:1512.03547 [cs.DS].
- [35] Daniel Andrén and Klas Markström, “The bivariate Ising polynomial of a graph,” *Discrete Appl. Math.* **157**, 2515–2524 (2009).
- [36] Masaki Ohkuwa, Hidetoshi Nishimori, and Daniel A. Lidar, “Reverse annealing for the fully connected p - spin model,” *Physical Review A* **98**, 022314 (2018), arXiv:1806.02542 [quant-ph].
- [37] Klas Markström, “From the Ising and Potts models to the general graph homomorphism polynomial,” in *Graph polynomials*, Discrete Math. Appl. (Boca Raton) (CRC Press, Boca Raton, FL, 2017) pp. 123–138.
- [38] Klas Markström and John C. Wierman, “Aperiodic non-isomorphic lattices with equivalent percolation and random-cluster models,” *Electron. J. Combin.* **17**, Research Paper 48, 14 (2010).
- [39] Vicky Choi, “Minor-embedding in adiabatic quantum computation: I. the parameter setting problem,” *Quantum Information Processing* **7**, 193–209 (2008).

APPENDIX: CHOICE OF GRAPHS

We discuss the construction of pairs (or larger tuples) of non-isomorphic graphs that are co-Ising, i.e., have identical classical Ising spectra.

We first define the Ising polynomial, or partition function for the Ising model [35]:

$$Z(G, x, y) = \sum_{\vec{s} \in \Omega} x^{E(\vec{s})} y^{M_z(\vec{s})}, \quad (6)$$

where \vec{s} is a spin configuration, Ω is the space of all possible configurations, and $E(\vec{s})$ and $M_z(\vec{s})$ are the energy and magnetization of the configuration \vec{s} . Co-Ising graphs have the same Ising polynomial.

For small n (≤ 10), a full classification of equivalence classes of co-Ising graphs is known. The first such examples were given in Ref. [35], where they were found via a complete search of all small graphs, and the search was extended in Ref. [37], where non-isomorphic graphs which have the same partition function for all two-state spin models were found. But due to the rapidly growing number of non-isomorphic graphs, even when restricted to e.g. regular graphs, and the rarity of co-Ising pairs, any complete search will be limited to quite small sizes.

In Ref. [35] a technique was introduced for constructing large families of non-isomorphic graphs with the same Ising-polynomial. This method was extended in Ref. [38] to the random-cluster model. Using data from Refs. [35,

37] we use a simple version of this method to construct larger graphs to use as benchmarks.

This method makes use of the *rooted Ising-polynomial* $Z(G, v, x, y)$ of a graph G . Given a vertex v in the graph G this polynomial is defined as the usual Ising-polynomial except that we only sum over those states on G in which the spin of v is $+1$. Note that the full Ising-polynomial is given by $Z(G, x, y) = Z(G, v, x, y) + Z(G, v, x, 1/y)$. So, if two graphs G_1, G_2 have the same rooted polynomials $Z(G_1, v_1, x, y)$ and $Z(G_2, v_2, x, y)$ for some vertex $v_1 \in G_1$ and $v_2 \in G_2$ then they will have the same Ising-polynomial, but two graphs may have the same Ising-polynomial even if no such pair of vertices exist.

The rooted polynomial has the useful property that if we start with any two graphs, and root vertices v_1 and v_2 , and build a new graph G_3 by identifying the vertices v_1 and v_2 into a new vertex v_3 then

$$Z(G_3, v_3, x, y) = Z(G_1, v_1, x, y)Z(G_2, v_2, x, y)/y.$$

So, if we know the rooted polynomial for the smaller graphs G_1 and G_2 we can easily find the full Ising-polynomial of G_3 , and if we start with two different pairs of non-isomorphic graphs with the same rooted polynomials we can build two larger graphs which are Co-Ising, but which may not be isomorphic. Similarly we can use more than two graphs in this product, as long as we divide by the right power of y .

Using the examples from Ref. [37] we search for pairs of graphs with the same rooted polynomials. Several such pairs exist, and we opt for a few pairs of tree-like starting graphs to keep them native to the Chimera architecture. While minor embedding [39] is a commonly used technique for dealing with non-native graphs, where several physical qubits linked by strong ferromagnetic couplings are used to represent a single node from the original graph, we avoid it for the present study.

All the tested graphs are listed below:

$$G13 = [(1, 8), (1, 10), (1, 11), (1, 13), (2, 9), (2, 11), (2, 13), (3, 10), (3, 13), (4, 10), (5, 11), (6, 12), (7, 12), (9, 12), (12, 13)]$$

$$G13p = [(1, 8), (1, 10), (1, 11), (1, 13), (2, 9), (2, 11), (2, 13), (3, 10), (3, 11), (4, 10), (5, 12), (6, 12), (7, 13), (8, 12), (12, 13)]$$

$$G17 = [(1, 2), (1, 3), (1, 4), (1, 5), (4, 6), (4, 7), (5, 8), (5, 9), (5, 10), (6, 11), (10, 12), (10, 13), (10, 14), (11, 15), (11, 16), (12, 17)]$$

$$G17p = [(1, 2), (1, 3), (1, 4), (1, 5), (4, 6), (5, 7), (5, 8), (5, 9), (6, 10), (6, 11), (9, 12), (9, 13), (9, 14), (10, 15), (12, 16), (12, 17)]$$

$$G25p1 = [(1, 6), (1, 7), (3, 7), (4, 8), (4, 9), (5, 8), (5, 9), (6, 9), (10, 14), (10, 15), (11, 15), (12, 16), (12, 17), (13, 16), (13, 17), (14, 17), (18, 22), (18, 23), (19, 23), (20, 24), (20, 25), (21, 24), (21, 25), (22, 25), (2, 6), (2, 14), (2, 22)]$$

$$G25p2 = [(1, 6), (1, 7), (3, 7), (4, 8), (4, 9), (5, 8), (5, 9), (6, 9), (10, 14), (10, 15), (11, 15), (12, 16), (12, 17), (13, 16), (13, 17), (14, 17), (18, 23), (18, 25), (19, 22), (19, 24), (20, 23), (20, 25), (21, 24), (21, 25), (2, 6), (2, 14), (2, 18)]$$

$$G25p3 = [(1, 6), (1, 7), (3, 7), (4, 8), (4, 9), (5, 8), (5, 9), (6, 9), (10, 15), (10, 17), (11, 14), (11, 16), (12, 15), (12, 17), (13, 16), (13, 17), (18, 23), (18, 25), (19, 22), (19, 24), (20, 23), (20, 25), (21, 24), (21, 25), (2, 6), (2, 10), (2, 18)]$$

$$G25p4 = [(1, 7), (1, 9), (2, 6), (2, 8), (3, 7), (3, 9), (4, 8), (4, 9), (10, 15), (10, 17), (11, 14), (11, 16), (12, 15), (12, 17), (13, 16), (13, 17), (18, 23), (18, 25), (19, 22), (19, 24), (20, 23), (20, 25), (21, 24), (21, 25), (5, 1), (5, 10), (5, 18)]$$

$$G27 = [(1, 14), (1, 17), (2, 14), (2, 22), (3, 4), (3, 5), (4, 10), (4, 12), (5, 11), (5, 13), (6, 7), (6, 8), (6, 15), (7, 10), (7, 11), (8, 12), (8, 13), (9, 12), (9, 13), (9, 14), (10, 15), (11, 15), (14, 15), (16, 17), (16, 21), (17, 18), (18, 19), (19, 20), (20, 21), (22, 23), (22, 27), (23, 24), (24, 25), (25, 26), (26, 27)]$$

$$G27p = [(1, 14), (1, 17), (2, 14), (2, 23), (3, 4), (3, 5), (4, 10), (4, 11), (5, 12), (5, 13), (6, 7), (6, 8), (6, 15), (7, 10), (7, 12), (8, 11), (8, 13), (9, 12), (9, 13), (9, 14), (10, 15), (11, 15), (14, 15), (16, 17), (16, 21), (17, 18), (18, 19), (19, 20), (20, 21), (22, 23), (22, 27), (23, 24), (24, 25), (25, 26), (26, 27)]$$

$$G33 = [(1, 6), (1, 7), (3, 7), (4, 8), (4, 9), (5, 8), (5, 9), (6, 9), (10, 14), (10, 15), (11, 15), (12, 16), (12, 17), (13, 16), (13, 17), (14, 17), (18, 22), (18, 23), (19, 23), (20, 24), (20, 25), (21, 24), (21, 25), (22, 25), (26, 30), (26, 31), (27, 31), (28, 32), (28, 33), (29, 32), (29, 33), (30, 33), (2, 6), (2, 14), (2, 22), (2, 30)]$$

$$G33p = [(1, 6), (1, 7), (3, 7), (4, 8), (4, 9), (5, 8), (5, 9), (6, 9), (10, 14), (10, 15), (11, 15), (12, 16), (12, 17), (13, 16), (13, 17), (14, 17), (18, 22), (18, 23), (19, 23), (20, 24), (20, 25), (21, 24), (21, 25), (22, 25), (26, 31), (26, 33), (27, 30), (27, 32), (28, 31), (28, 33), (29, 32), (29, 33), (2, 6), (2, 14), (2, 22), (2, 26)]$$

$$G33p1 = [(1, 6), (1, 7), (3, 7), (4, 8), (4, 9), (5, 8), (5, 9), (6, 9), (10, 15), (10, 17), (11, 14), (11, 16), (12, 15), (12, 17), (13, 16), (13, 17), (18, 23), (18, 25), (19, 22), (19, 24), (20, 23), (20, 25), (21, 24), (21, 25), (26, 31), (26, 33), (27, 30), (27, 32), (28, 31), (28, 33), (29, 32), (29, 33), (2, 6), (2, 10), (2, 18), (2, 26)]$$

$$G33p2 = [(1, 6), (1, 7), (2, 6), (3, 7), (4, 8), (4, 9), (6, 9), (10, 15), (10, 17), (11, 14), (11, 16), (12, 15), (12, 17), (13, 16), (13, 17), (18, 23), (18, 25), (19, 22), (19, 24), (20, 23), (20, 25), (21, 24), (21, 25), (26, 31), (26, 33), (27, 30), (27, 32), (28, 31), (28, 33), (29, 32), (29, 33), (5, 8), (5, 9), (5, 10), (5, 18), (5, 26)]$$